Modeling of a Planar Motion Stage for Precision Positioning

Kai Treichel**, Remon Al Azrak*, Johann Reger*, and Kai Wulff*

***Abstract*— In this contribution we develop a physical model for a non contact, high-precision Lorentz force planar motion stage of linear DC brushless type. We derive physical models of the relevant components and investigate sources and influences of various parasitic effects and disturbances. For the latter, phenomenological models are developed that capture the behavior observed throughout experiments. The position dependency of the Lorentz forces is reduced by a minimum power commutation. Finally, model characteristics and parameters are identified from experimental test rig data.**

I. INTRODUCTION

The emergence and steady growth of nanotechnology for now more than 30 years has not only enriched numerous fields in technology but also daily life. Many applications such as scanning probe/force microscopy, lithography in semiconductor and microelectronic device fabrication, laser cutting in precision machining require submicron to nanometer positioning accuracy and high repeatability while performing complex trajectory tracking tasks at high speed [1].

For meeting these challenges and still increasing requirements various linear/planar electromagnetic actuators evolved in the past decades. They range from planar motor concepts such as the sawyer planar stepper motor (1968) used in semiconductor manufacturing (operated in open-loop), to rotary linear drives, planar induction motors, non contact planar brushless DC or Lorentz motors, and piezoelectric drives that are operated in closed-loop (see survey in [2]).

In joint research together with the planar motor manufacturer TETRA[1] we concentrate on deriving a thorough but yet simple simulation model for the control of an aerostatic levitated planar Lorentz motor of linear DC brushless type, similar to those in [3]–[7]. In the context of these motors (matched) input disturbances are one of the major challenges for position control. These disturbances often originate from force ripples [8] that occur at the control input when subject to model uncertainties, i.e. commutation errors [9], [10], asymmetries and offsets in power amplifiers [9], magnetization effects of ferrous components in the traversing range (cogging-forces) [8], current ripple due to PWM-power-amplifiers [8], eddy current damping effects, spring force effects of air supply hoses and downhill-slope forces due to an inaccurate stator adjustment, undesired coupling effects between motion axes as well as parameter variations caused by load changes and different ambient temperatures.

*All authors are with Control Engineering Group, Technische Universität Ilmenau, P.O. Box 10 05 65, D-98684, Ilmenau, Germany

**Author for correspondence: kai.treichel@tu-ilmenau.de

[1]TETRA Gesellschaft für Sensorik, Robotik und Automation mbH, Gewerbepark Am Wald 4, D-98693 Ilmenau, Germany.

This paper is a first step towards developing robust tracking controllers in the diverse applications of such machines. Therefore it is indispensable that the model reflects the main challenges for control, i.e. through the aid of realistic disturbance models that can be used for the assessment of advanced control techniques. Thus the model shall encompass all the prominent dynamics and the most significant parasitic effects/disturbances so as to learn the structural properties of the system and disturbances—especially where the disturbances affect the system.

II. OPERATION PRINCIPLE

As illustrated in Fig. 1 the planar motion stage essentially consists of a passive moving element and an active non moving part. A rigid aluminum plate acts as the movable part (mover) of the motor that may be positioned in three degrees of freedom (DOF) in the plane: two translational x, y and one rotational ϕ. The mover is equipped with permanent magnet arrays (PMAs), hence passive, and suspended by pressurized air employing aerostatic suspension bearings. This avoids dry friction and in particular stick-slip-effects such that smooth and nearly frictionless motion in the plane is possible. The stator part of the machine is a massive base unit made of granite which comprises four permanently fixed two-phase-coil-systems arranged in a crosswise manner.

If current is applied to the coils, both the coils and the permanent magnets (PMs) interact with each other. As a consequence the forces and torques (F_x, F_y, M_z) are exerted on the mover accelerating it along its motion-axes (x, y, ϕ) (see Fig. 2). In accordance to Lorentz' Law the forces and torques exerted are proportional to the current applied. They act perpendicular with respect to the direction of current flow as well as perpendicular to the magnetic field direction.

In order to control the phase currents considered as control inputs four PWM two-phase digital current amplifiers (DCAs) are employed as servo-amplifiers for the corresponding two-phase-coil-systems (cf. Fig. 2). Intuitively such a PMA-coil-combination can be regarded as a linear motor (LM), as discussed on several publications, e.g. [4], [6], [7], [11]. Thus we call a DCA-LM-combination a linear servomotor. Please note that the architecture described above is widely used and similar to other motor concepts reported in the literature (see e.g. [3]–[7], [11]).

For clarity, we denote the elements of the four linear servomotors that produce thrust forces in the x- and y-directions by X_i and Y_i, resp., where $i = 1, 2$ serves as system index. Note that the motors (X_1, X_2) such as (Y_1, Y_2) oppose each other. Usually the LM pair (X_1, X_2) is driven simultaneously in order to achieve symmetric movement in

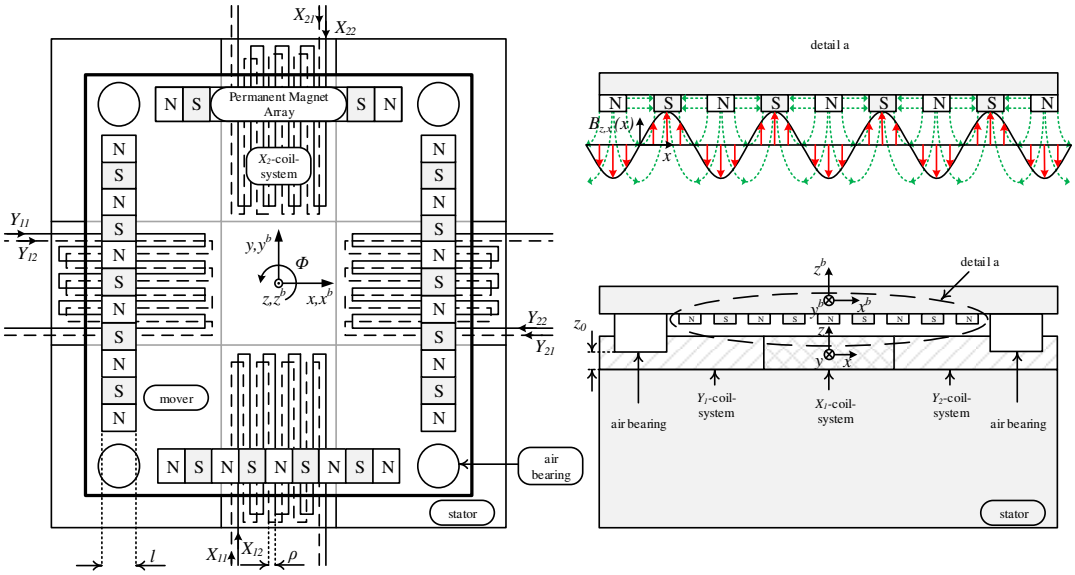

Fig. 1. Top view of motion stage (left), side view of X_1-permanent magnet array (PMA) (top right) with magnetic field lines (green), vertical vector components of the flux density (red) and sinusoidal magnitude of the vertical vector components (black). Side view of motion stage (bottom right).

the direction of x. The same applies to the LMs (Y_1, Y_2). The phase index $j = 1, 2$ in X_{ij} and Y_{ij} is to represent the j-th phase of the i-th LM, coil-system or DCA. Accordingly, the eight real-valued scalar coil phase currents are expressed by $i_{x_{ij}}(t)$ and $i_{y_{ij}}(t)$. They are measured and driven to the reference trajectories $i^r_{x_{ij}}(t)$ and $i^r_{y_{ij}}(t)$ by the DCAs.

The mover's motion is described in an inertial coordinate frame (i-frame) (x, y, z) located at the center of the stator surface and a body-fixed frame (b-frame) (x^b, y^b, z^b) coincident with the center of gravity (CG) and principle axes of rotation (Fig. 1). The position coordinates x and y of the movers' CG and its yaw angle ϕ are measured with an optical, incremental sensor underneath the mover.

Fig. 2 shows a typical control task, where a reference $\tau^r(t) = \left(F^r_x(t), F^r_y(t), M^r_z(t)\right)^{\mathrm{T}}$ is specified for the generalized forces $\tau(t) = \left(F_x(t), F_y(t), M_z(t)\right)^{\mathrm{T}}$ on the mover such that its position $q(t) = \left(x(t), y(t), \phi(t)\right)^{\mathrm{T}}$ tracks a desired reference trajectory $q^r(t) = \left(x^r(t), y^r(t), \phi^r(t)\right)^{\mathrm{T}}$. A motor commutation law maps the desired reference $\tau^r(t)$ to the corresponding phase current reference $i^r(t) = \left(i^r_{x11}(t), i^r_{x12}(t), \ldots, i^r_{y21}(t), i^r_{y22}(t)\right)^{\mathrm{T}}$. The current control loop of the DCAs assures $i(t) \to i^r(t)$ for the measured current $i(t) = \left(i_{x11}(t), i_{x12}(t), \ldots, i_{y21}(t), i_{y22}(t)\right)^{\mathrm{T}} \in \mathbb{R}^8$. Through the electromagnetic coupling of forces, from $i(t) \to i^r(t)$ we have $\tau(t) \to \tau^r(t)$, thus $q(t) \to q^r(t)$, as desired.

III. MODELING

A. Actuator Dynamics

The four LMs form the actuating elements of the motion stage. For the actuation of the mover it is fundamental that the phases of each coil system are shifted by $\rho = \frac{\pi}{2}$ (Fig. 1). Remarkably, the two-phase coil-systems of the actuators are built in printed circuit board (PCB) construction, allowing cost-effective and compact motor design with fewer components and faster assembly. A downside of the construction, however, is the mutual induction when a current is applied to either one or both of the coil phases. This is due to the fact that the phases lie nearby and even overlap.

Taking into account induction of the neighboring phases, the voltage across the coils of the X_1-coil-system reads

$$u_{x_{1j}}(t) = R_{x_{1j}}\, i_{x_{1j}}(t) + \dot{\Psi}_{x_{1j}}(i_{x_{11}}, i_{x_{12}}, x), \qquad (1)$$

for $j = 1, 2$ and where $R_{x_{1j}} \in \mathbb{R}_+$ denotes the respective phase winding resistance and $\Psi_{x_{1j}}(i_{x_{11}}, i_{x_{12}}, x) \in \mathbb{R}$ is the magnetic flux linking the adjacent windings (see [10], [12]). The magnetic flux depends on the phase currents $i_{x_{1j}} \in \mathbb{R}$ as well as on the position dependent magnetic flux density of the PMA above the coil.

Computing the rate of $\Psi_{x_{1j}}(i_{x_{11}}, i_{x_{12}}, x)$ and noticing that the flux is linear in the currents [10], [13], eqn. (1) turns to

$$u_{x_{11}} = R_{x_{11}}\, i_{x_{11}} + L_{x_{11}} \frac{di_{x_{11}}}{dt} + M^{x_1}_{21} \frac{di_{x_{12}}}{dt} + \frac{\partial \Psi_{x_{11}}}{\partial x}\, \dot{x} \qquad (2)$$

$$u_{x_{12}} = R_{x_{12}}\, i_{x_{12}} + L_{x_{12}} \frac{di_{x_{12}}}{dt} + M^{x_1}_{12} \frac{di_{x_{11}}}{dt} + \frac{\partial \Psi_{x_{12}}}{\partial x}\, \dot{x}, \qquad (3)$$

where $L_{x_{1j}} \in \mathbb{R}_+$ denotes self inductances and $M^{x_1}_{21}, M^{x_1}_{12} \in \mathbb{R}_+$ the mutual inductances of either phase of the X_1-coil.

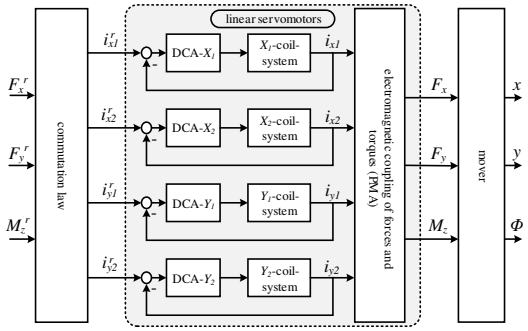

Fig. 2. Signal flow diagram of the motion stage, where the quantities $i_{x_i} = (i_{x_{i1}}, i_{x_{i2}})^{\mathrm{T}}$ and $i_{y_i} = (i_{y_{i1}}, i_{y_{i2}})^{\mathrm{T}}$ while $i = 1, 2$ are vectors of the corresponding phase currents. The same applies to $i^r_{x_i}$ such as $i^r_{y_i}$.

The first terms account for ohmic losses whereas the second and the third represent the coil's self and mutual induction. The last terms model the back-emf that occurs when the PMAs of the mover move above the coils. Note that $\partial\Psi_{x_{1j}}/\partial x = \bar{l}_{x_{1j}} B_{x_{1j}}(x) = K_{x_{1j}}(x)$ with $B_{x_{1j}}(x)$ as the magnitude of the flux density of the PMA and $\bar{l}_{x_{1j}}$ the effective length of the corresponding phase winding within the magnetic field. The voltage induced from the back-emf is $-\bar{l}_{x_{1j}} B_{x_{1j}}(x)\,\dot{x}$, as exposed in [12], [13], but here with position dependent flux density.

For a compact notation we introduce $i_{x_1} = (i_{x_{11}}, i_{x_{12}})^{\mathrm{T}}$ and $u_{x_1} = (u_{x_{11}}, u_{x_{12}})^{\mathrm{T}}$ and rewrite (2) and (3) in the form

$$\tilde{L}_{x_1} \frac{di_{x_1}(t)}{dt} = u_{x_1}(t) - R_{x_1}\, i_{x_1}(t) - K_{x_1}(x)\,\dot{x}(t) \qquad (4)$$

with resistance matrix $R_{x_1} = \mathrm{diag}(R_{x_{11}}, R_{x_{12}})$ and vector $K_{x_1}(x) = (K_{x_{11}}(x), K_{x_{12}}(x))^{\mathrm{T}}$ accounting for the back-emf, and the generalized inductance matrix

$$\tilde{L}_{x_1} = \begin{pmatrix} L_{x_{11}} & M_{21}^{x_1} \\ M_{12}^{x_1} & L_{x_{12}} \end{pmatrix}. \qquad (5)$$

Doing so for X_2, Y_1 and Y_2 and combining the results yields

$$\tilde{L} \frac{di(t)}{dt} = u(t) - R\, i(t) - K(q)\,\dot{q}(t), \qquad (6)$$

where $u = (u_{x_{11}}, u_{x_{12}}, \ldots, u_{y_{21}}, u_{y_{22}})^{\mathrm{T}} \in \mathbb{R}^8$ is the input voltage, $\tilde{L} = \mathrm{diag}(\tilde{L}_{x_1}, \ldots, \tilde{L}_{y_2}) \in \mathbb{R}_+^{8\times 8}$ and $R = \mathrm{diag}(R_{x_1}, \ldots, R_{y_2}) \in \mathbb{R}_+^{8\times 8}$ are block diagonal matrices, and

$$K(q) = \begin{pmatrix} K_{x_1}(x) & 0 & 0 \\ K_{x_2}(x) & 0 & 0 \\ 0 & K_{y_1}(y) & 0 \\ 0 & K_{y_2}(y) & 0 \end{pmatrix} \in \mathbb{R}^{8\times 3}. \qquad (7)$$

The phase currents of the respective coil-systems are controlled by switched DCAs with fixed current control architecture. For gaining insights in the transient behavior, we model the closed loop consisting of the DCAs and coils.

The DCAs' current control loop consists of a multivariable moving average filter of order $N = 8$ located in the feedback and a multivariable discrete PI-controller (velocity algorithm) in ISA-form. The filter aims to remove PWM induced current ripple from the measured (sampling time T) A/D converted phase currents $y_k = i(kT) \in \mathbb{R}^8$ (neglecting quantization) so as to improve the current signals $\bar{y}_k \in \mathbb{R}^8$ for the control. The filter and controller are given by the discrete-time system

$$\bar{y}_k = \tfrac{1}{N+1}\,(y_k + y_{k-1} + \cdots + y_{k-N}) \qquad (8)$$

$$\bar{u}_k = \bar{u}_{k-1} - K_p\,(\bar{y}_k - \bar{y}_{k-1}) + K_i\,T_a\,(\bar{r}_k - \bar{y}_k), \qquad (9)$$

where $r_k = i^r(kT) \in \mathbb{R}^8$ is the reference current, $\bar{u}_k \in \mathbb{R}^8$ the control signal, and $K_p \in \mathbb{R}^{8\times 8}$ as well as $K_i \in \mathbb{R}^{8\times 8}$ are the (diagonal) controller gain matrices. Note that $\bar{r}_k = f(r_k)$ is a modification of r_k by some function $f : \mathbb{R}^8 \to \mathbb{R}^8$ for casting nonlinear steady state behavior into a Hammerstein model with static input nonlinearity and LTI dynamics.

Since the amplifiers are PWM-switched with 200 kHz the current ripple is moderate. Focusing on the average transient behavior we model them as ideal continuous voltage amplifiers with gain $K_T \in \mathbb{R}^{8\times 8}$. Thus, we have the continuous

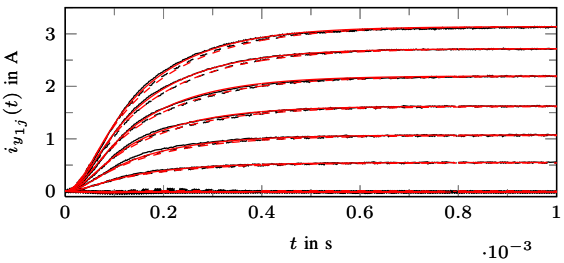

Fig. 3. Comparison of model (red) with measured (black) current transient response of phases 1 (solid) and 2 (dashed) of LM Y_1.

coil input voltage $u(t) = K_T\,\bar{u}(t)$, where $\bar{u} \in \mathbb{R}^8$ is the average continuous time signal of the PWM control $\bar{u}_k$.

Fig. 3 compares simulations with experiments on LM Y_1 via measured transient current responses on reference current steps from 0.5 A to 3 A (in 0.5 A steps over the current range of the DCAs). The model matches the transient behavior well. The quantity $f(r_k)$ obtained from measurement data, serves to adjust the DC gain. Linear regression yields

$$\bar{r}_k = f(r_k) = \epsilon\, r_k + \sigma, \qquad (10)$$

with $\epsilon \approx 1.08$ for all phases and $\sigma \in \mathbb{R}^8$ small, componentwise. The observed behavior can be traced back to temperature drifts and inaccurate current measurements.

For point-to-point position control of the mover, the DC-gain is not critical because the plant shows integral behavior. In similar cascade control settings, e.g. for the position or the angular velocity control of DC-motors, even simpler P-controllers are used for the current loop (see [13]) as the main purposes of the current controller are: speeding up the response by forcing the current to flow in the right direction, decoupling the phases from each other, i.e. rejecting the mutual induction, and suppressing the effects of output disturbances (back-emf). These requirements are met by the DCAs' current control loop. For trajectory tracking control, however, the DC-gain (ϵ) has to be known for the inversion. The affine term σ such as all asymmetries regarding the coils that oppose each other cause undesired force ripple and torques respectively (c.f. III-E).

As the closed-loop dynamics of the DCAs and coils are very fast compared to the mover dynamics (a mass with 20 kg) and since the requirements of decoupling and back-emf suppression are met, we may neglect the current loop dynamics and just consider the static relationship

$$\lim_{k\to\infty} y_k = \bar{r}_k = \epsilon\, r_k + \sigma \;\Leftrightarrow\; i(kT) = \epsilon\, i^r(kT) + \sigma\,. \qquad (11)$$

Due to the small sampling time, $T = 5\,\mu$s, of the DCAs the static DCA-coil-model is treated as continuous:

$$i(t) = \epsilon\, i^r(t) + \sigma. \qquad (12)$$

B. Magnetic Flux Density, Lorentz-Forces and Torques

The geometry of the PMAs is designed (via FEM analysis) such that the magnitude of the vertical components of the magnetic flux density wrt. the x- and y-positions describe a sinusoid (Fig. 1 detail a), simplifying electronic commutation. We confine the description on vertical components since only these generate the planar propulsion forces in the

(x, y)-plane. Also, analysis is restricted on a constant flight height z_0. The magnetic field is subject to the assumptions:

Assumption 1 *The vertical flux density $B_{x_{ij}}(x, z)$ of $B_{z,x}(x, y, z)$ above the X_{ij}-coil is constant along the y-axis.*

Assumption 2 *The vertical flux density $B_{y_{ij}}(y, z)$ of $B_{z,y}(x, y, z)$ above the Y_{ij}-coil is constant along the x-axis.*

Along with [14], [10] we consider an exponential dependency on the flight height z. For constant $z = z_0$, we have

$$B_{x_{ij}}(x, z_0) = \hat{B}\, e^{-\alpha z_0} \sin(\tfrac{2\pi}{T_m} x + \rho_j + \varphi_x) \tag{13}$$

$$B_{y_{ij}}(y, z_0) = \hat{B}\, e^{-\alpha z_0} \sin(\tfrac{2\pi}{T_m} y + \rho_j + \varphi_y) \tag{14}$$

with $\bar{B} = \hat{B}\, e^{-\alpha z_0}$ the amplitude with remanence $\hat{B} > 0$, $\alpha > 0$ a geometry-dependent constant, $T_m > 0$ the magnet period, $\rho_j = \frac{\pi}{2}(j-1)$ the displacement of the adjacent phases (phase pitch), and $\varphi_x, \varphi_y > 0$ phase shifts wrt. the i-frame.

In general, the 3d Lorentz force $\mathcal{F}$ of an energized coil in a magnetic field with flux density $\mathcal{B} \in \mathbb{R}^3$ results from

$$\mathcal{F} = \mathcal{I} \int_C dl \times \mathcal{B} \tag{15}$$

evaluated over the wire length C of the coil in direction of the current $\mathcal{I}\, dl$, see [12]. The Lorentz forces of the planar motor are modeled under the assumptions:

Assumption 3 *The coils wrt. the x- and y-axes are placed orthogonally. Coils are assumed long wrt. the PM width l, excluding boundary effects, and have a current flow direction within the magnetic field orthogonal to the x- and y-axis.*

Assumption 4 *The mover's roll, pitch and yaw motion is small s.t. its influence on the electromagnetic forces is negligible. For the maximum yaw angle $\phi_{max} \in [-0.25°, 0.25°]$ with roll and pitch angles in between $\pm 0.01°$. Therefore, $(B_{x_{ij}}(x), B_{y_{ij}}(y))$ of the magnetic field are perpendicular to resp. coil surfaces, hence, also to every single coil winding.*

These assumptions imply that the Lorentz forces are acting in x and y direction only, perpendicularly wrt. the coil (windings), regardless of the mover's orientation ϕ (Fig. 4). Thus, the forces in x and y direction are decoupled from one another. With Assumption 3 and with $\bar{l}_{x_{ij}} e_y \in \mathbb{R}^3$ and $\bar{l}_{y_{ij}} e_x \in \mathbb{R}^3$ solutions of the line integral representing the effective lengths of the dedicated coil phases within the magnetic field, the electromagnetic forces between the PMAs and the single coil phases read

$$F_{x_{ij}}(x) = i_{x_{ij}} \bar{l}_{x_{ij}} e_y \times B_{x_{ij}}(x) e_z = i_{x_{ij}} \bar{l}_{x_{ij}} B_{x_{ij}}(x) e_x \tag{16}$$

$$F_{y_{ij}}(y) = i_{y_{ij}} \bar{l}_{y_{ij}} e_x \times B_{y_{ij}}(y) e_z = i_{y_{ij}} \bar{l}_{y_{ij}} B_{y_{ij}}(y) e_y, \tag{17}$$

where $e_x, e_y, e_z \in \mathbb{R}^3$ are the unit vectors. Note that solving the line integral is not necessary, since the motor constants $K_{mx_{ij}} = \bar{l}_{x_{ij}} \bar{B}$ are obtained experimentally. Thus, the total sums of forces in the respective directions are

$$F_x = \textstyle\sum_{i,j=1}^{2} F_{x_{ij}}, \quad F_y = \textstyle\sum_{i,j=1}^{2} F_{y_{ij}} \tag{18}$$

(see Fig. 4), whereas that of the torques around the z-axis is

$$M_z = d_2 \textstyle\sum_{i,j=1}^{2} F_{y_{ij}} (-1)^i - d_1 \sum_{i,j=1}^{2} F_{x_{ij}} (-1)^i, \tag{19}$$

with d_1, d_2 distances from the mover's CG to the center line of the PMAs. We drop the dependency on ϕ in d_1, d_2 since $|\phi_{\max}|$ is small. For brevity, we omit the dependencies in forces and torques on currents and positions, resp.

Expressing $\tau = (F_x, F_y, Mz)^{\mathrm{T}}$ with $i_{x_{ij}}$ and $i_{y_{ij}}$ yields

$$\tau = B(q)\, i \tag{20}$$

where

$$B(q)^{\mathrm{T}} = \begin{pmatrix} K_{mx} \sin(\zeta_x) & 0 & d_1 K_{mx} \sin(\zeta_x) \\ K_{mx} \cos(\zeta_x) & 0 & d_1 K_{mx} \cos(\zeta_x) \\ K_{mx} \sin(\zeta_x) & 0 & -d_1 K_{mx} \sin(\zeta_x) \\ K_{mx} \cos(\zeta_x) & 0 & -d_1 K_{mx} \cos(\zeta_x) \\ 0 & K_{my} \sin(\zeta_y) & -d_2 K_{my} \sin(\zeta_y) \\ 0 & K_{my} \cos(\zeta_y) & -d_2 K_{my} \cos(\zeta_y) \\ 0 & K_{my} \sin(\zeta_y) & d_2 K_{my} \sin(\zeta_y) \\ 0 & K_{my} \cos(\zeta_y) & d_2 K_{my} \cos(\zeta_y) \end{pmatrix} \tag{21}$$

is the control allocation matrix that expresses the position dependency of the field and the electromagnetic coupling of forces. Note that $\forall i, j$ the motor constants $K_{mx} = K_{mx_{ij}} = \bar{l}_{x_{ij}} \bar{B}$ as well as $K_{my} = K_{my_{ij}} = \bar{l}_{y_{ij}} \bar{B}$, while $\zeta_x = \frac{2\pi}{T_m} x + \varphi_x$ and $\zeta_y = \frac{2\pi}{T_m} y + \varphi_y$.

Though often not made explicit, assumptions 1–4 are standard and partially may be found in [11], [6], [5], [4].

C. Commutation Law

The previous analysis shows that the electromagnetic forces/torques (20) depend on the position. Furthermore, in view of the control task of Fig. 2 (Section II) we favor to specify reference forces τ^r rather than reference currents i^r (actual control inputs). These issues are resolved with the so-called motor commutation law $i^r = C_o(q)\, \tau^r$ that distributes the phase currents for obtaining the desired force independent from the mover position[2]. In fact, composing the commutation law and the control allocation (20) indicates that the commutation law results from inversion of $B(q)$.

Since the system is *overactuated* with 8 control inputs for 3 degrees of freedom, we follow the ideas of [15] for deriving a minimum power commutation law. To this end, we minimize the electric power $\|i\|^2 = i_{x_{11}}^2 + \ldots + i_{y_{22}}^2$ subject to $B\, i = \tau$, see [15]. The classical solution reads

$$i^r(t) = B(q)^{\mathrm{T}} \left(B(q) B(q)^{\mathrm{T}}\right)^{-1} \tau^r(t) = C_o(q)\, \tau^r(t). \tag{22}$$

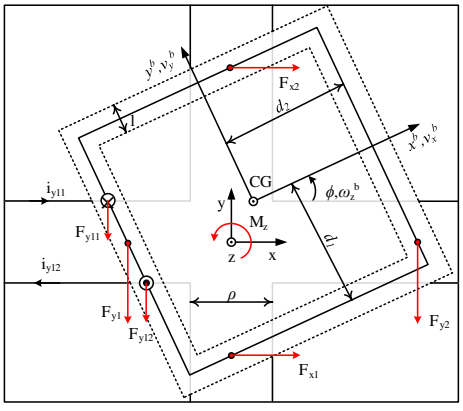

Fig. 4. Planar electromagnetic forces/torques on the mover: For simplicity, coil phases are depicted as conductors. Dotted lines indicate the location of the PMAs, the solid line spots the line of the applied electromagnetic forces. Forces $F_{x_i} = F_{x_{i1}} + F_{x_{i2}}$ act between the corresponding two coil phases, similarly F_{y_i}. Quantities v_x^b, v_y^b, ω_z^b are longitudinal, transversal and angular (around the z-axis) body velocities wrt. i-frame.

[2]This includes that the flux density is a pure sinusoid as in (13) and (14), the motor constants K_{mx}, K_{my} are perfectly known, and the static behavior of the current loop has parameters $\epsilon = 1$ and $\sigma = 0$.

It turns out that the minimum power commutation coincides with the well-known sine-cosine-commutation in motion control and electric machine engineering [9], [10], [15].

D. Mechanical Equations of Motion

We refer to [16] for the mover's mechanical equations of motion. This includes the velocity transformation

$$\dot{q}(t) = R(\phi)\,\nu(t), \tag{23}$$

and the well-known Newton-Euler-equations in b-frame

$$m\,(\dot{v}_c(t) + \omega(t) \times v_c(t)) = f_c(t) \tag{24}$$

$$I_c\,\dot{\omega}(t) + \omega(t) \times (I_c\,\omega(t)) = m_c(t) \tag{25}$$

In these equations, $\dot{q} \in \mathbb{R}^3$ is the velocity in i-frame and

$$R(\phi) = \begin{pmatrix} \cos(\phi) & -\sin(\phi) & 0 \\ \sin(\phi) & \cos(\phi) & 0 \\ 0 & 0 & 1 \end{pmatrix} \in \mathrm{SO}(3) \tag{26}$$

is an orthogonal matrix transforming b-frame velocity $\nu = (v_x^b, v_y^b, \omega_z^b)^{\mathrm{T}}$ into i-frame (Fig. 4), and $v_c = (v_x^b, v_y^b, 0)^{\mathrm{T}}$, $\omega = (0, 0, \omega_z^b)^{\mathrm{T}}$, $f_c = (f_x^b, f_y^b, 0)^{\mathrm{T}}$, $m_c = (0, 0, m_z^b)^{\mathrm{T}}$ are linear velocity, angular velocity, propelling forces and torques of the mover, resp., all defined in b-frame. Moreover, m and $I_c \in \mathbb{R}^{3\times3}$ are the mover's mass and inertia tensor. Assumption 4 and planar motion imply the zeros in ω, m_c, v_c and f_c. Since the b-frame origin coincides with the CG and the principle axes of rotation [16], the inertia tensor I_c is diagonal. Inserting v_c, ω, f_c and m_c in (24), (25) and enhancement by a linear damping $\tau_d^b(t) = -D\,\nu(t)$ yields

$$M\,\dot{\nu}(t) + C(\nu)\,\nu(t) + D\,\nu(t) = \tau^b(t) \tag{27}$$

as the dynamics in b-frame coordinates with

$$M = \begin{pmatrix} m & 0 & 0 \\ 0 & m & 0 \\ 0 & 0 & I_z \end{pmatrix},\; C(\nu) = \begin{pmatrix} 0 & -m\,\omega_z^b(t) & 0 \\ m\,\omega_z^b(t) & 0 & 0 \\ 0 & 0 & 0 \end{pmatrix} \tag{28}$$

as mass and Coriolis matrix, resp., $D = \mathrm{diag}(\mu_x, \mu_y, \mu_\phi)$ the damping matrix and $\tau^b = (f_x^b, f_y^b, m_z^b)^{\mathrm{T}}$ forces/torque in b-frame. Inverting the velocity transformation and using

$$\dot{\nu}(t) = R^{-1}(\phi)\left(\ddot{q}(t) - \dot{R}(\phi)\,R^{-1}(\phi)\,\dot{q}(t)\right), \tag{29}$$

where $\dot{R}(\phi) = R(\phi)\,S(\omega)$ the dynamics of the mover can partially be expressed in the i-frame coordinates:

$$R^{-1}(\phi)\left(M\ddot{q}(t) + \bar{C}(\dot{q})\dot{q}(t) + D\dot{q}(t)\right) = \tau^b(t). \tag{30}$$

Note that the Coriolis term $\bar{C}(\dot{q}) = (mI - M)\,S(\dot{q}) \in \mathbb{R}^{3\times3}$ made up of I as identity matrix and the skew symmetric cross product operator $S(\dot{q})$ [16] vanishes. Note further that $S(\dot{q}) = \frac{1}{m}C(\dot{q})$ and $S(\omega) = \frac{1}{m}C(\nu)$ since $\dot{\phi} = \omega_z^b$ (see last row of $R(\phi)$).

As we have assumed that the electromagnetic forces always act perpendicularly to the coils (see Assumption 4 and Fig. 4) the forces propelling the mover act in i-frame. Their expression in b-frame requires the rotation $\tau^b = R^{-1}(\phi)\tau$. This finally yields the dynamics now in i-frame

$$M\ddot{q}(t) + D\dot{q}(t) = \tau(t) = B(q)\,i(t). \tag{31}$$

Note that for planar motion no gravitational terms occur. With (22) the right hand side of (31) becomes τ^r.

E. Phenomenological Disturbance Models

In general, the disturbances acting on the motion stage are characterized by the imperfectness of the magnetic field as well as external parasitic forces caused by magnetization and eddy current effects. Since numerical computation of the magnetic flux density distribution and magnetization effects is expensive we propose phenomenological models for the phenomena that have been observed throughout the measurements/experiments. Some typical disturbances in the context of planar motors are also presented in [8]–[10].

Firstly, commutation errors occur if the actual flux density distribution deviates from the theoretical design captured in $B(q)$. Fig. 5 shows an experimental flux density measurement (black), measured with a Hall effect sensor. Using

$$B_{x_{ij}}^p = \alpha_1 \tanh\left(\alpha_2\,\sinh(\alpha_3\,B_{x_{ij}}(x))\right) \tag{32}$$

$$B_{y_{ij}}^p = \alpha_1 \tanh\left(\alpha_2\,\sinh(\alpha_3\,B_{y_{ij}}(y))\right) \tag{33}$$

for matching the ideal flux density with the area/region on the top and around zero a very good model fit (red) with the real flux density is achieved. Inserting this magnetic field model in $B(q)$ yields the parasitic control allocation matrix $B^p(q)$ such that $\Delta B(q) = B^p(q) - B(q)$ may denote its deviation from the ideal description.

However, most significant is the influence from external forces due to magnetization-effects of ferrous components in the traversing range (see Fig. 7). Further external forces are spring forces of air supply hoses and downhill-slope forces due to an imprecise/inaccurate adjustment of the stator. A closed-loop experiment was conducted with the mover operated in constant velocity. We identified the external disturbances during the experiment through analysis of the

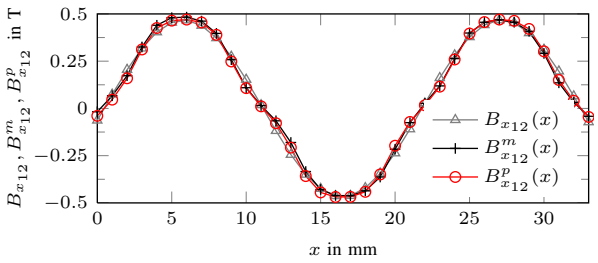

Fig. 5. Comparison of ideal $B_{x_{12}}$, measured $B_{x_{12}}^m$ and simulated $B_{x_{12}}^p$ magnetic flux density distributions of the X_1-PMA along the x-axis. $B_{x_{12}}(x) = \bar{B}\sin(\zeta_x)$, while the phenomenological magnetic flux model is given by $B_{x_{12}}^p(x) = \alpha_1 \tanh\left(\alpha_2\,\sinh(\alpha_3\,B_{x_{12}}(x))\right)$ with $\bar{B} = 0.4677$, $\alpha_1 = 0.4851$, $\alpha_2 = 0.1877$, $\alpha_3 = 6.6367$, $T_m = 21.3423$ and $\varphi_x = -0.1355$ obtained via curve fitting. The normalized root mean square error between measured and simulated distributions is 1.32%.

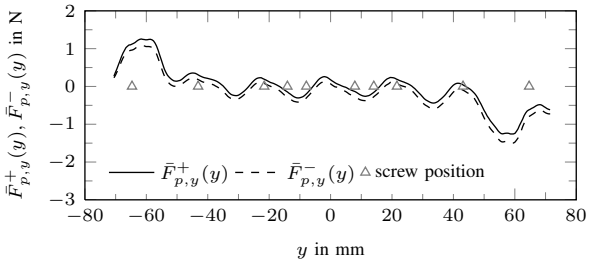

Fig. 6. Experimentally identified parasitic forces for $x, \phi \equiv 0$ and $y \in [-70, 70]$ mm due to magnetization of ferrous screws that fix the coils.

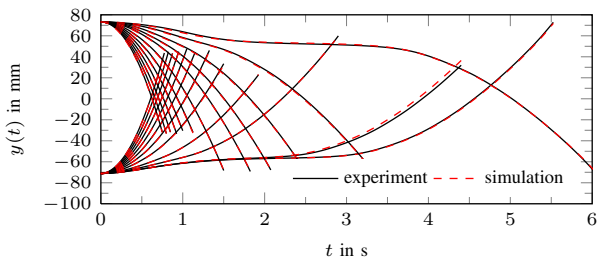

Fig. 7. Comparison of experimental position data with simulations on the proposed model for current/force step responses (in whole current/force range of 0–3 A, 0–10 N) over the entire traversing range along the y-axis.

control signal in a velocity controller as a measure of the external disturbances. Fig. 6 indicates a strong correlation between force ripple and coil-screw positions. The external parasitic forces are direction dependent and even scale with the magnitude of the velocity. In this regard, we propose the following phenomenological model for the x-direction:

$$F_{p,x}(x,\dot{x}) = \begin{cases} \mu_{p,x}\,\dot{x} + \bar{F}^{+}_{p,x}(x), & \text{for } \dot{x} \geq 0 \\ \mu_{p,x}\,\dot{x} + \bar{F}^{-}_{p,x}(x), & \text{for } \dot{x} < 0 \end{cases} \tag{34}$$

with direction dependent $\bar{F}^{+}_{p,x}(x)$ and $\bar{F}^{-}_{p,x}(x)$ (Fig. 6) and damping coefficient $\mu_{p,x} > 0$. For softer switching we use

$$\begin{aligned} F_{p,x}(x,\dot{x}) = \mu_{p,x}\,\dot{x} &+ \tfrac{1}{2}\left(\tanh(\delta\dot{x}) + 1\right)\,\bar{F}^{+}_{p,x}(x) \\ &- \tfrac{1}{2}\left(\tanh(\delta\dot{x}) - 1\right)\,\bar{F}^{-}_{p,x}(x) \end{aligned} \tag{35}$$

with $\delta > 0$ sufficiently large. Making use of (35) accordingly along the coordinates of y and ϕ we obtain the parasitic external forces/torques $\tau^p(q,\dot{q}) = (F_{p,x}, F_{p,y}, M_{p,\phi})^{\mathrm{T}}$.

The disturbance models combine to the perturbed system:

$$M\ddot{q}(t) + D\dot{q}(t) = \tau_{total}, \tag{36}$$

where $\tau_{total} = (B(q) + \Delta B(q))\,i(t) - \tau^p(q,\dot{q})$ results from (12) and (22) as per

$$\begin{aligned} \tau_{total} &= \epsilon\tau^r + \epsilon\Delta B C_o \tau^r + (B + \Delta B)\sigma - \tau^p \\ &= \epsilon\tau^r(t) + \underbrace{\tau^c(q) + \tau^o(q) - \tau^p(q,\dot{q})}_{d(q,\dot{q})} \end{aligned} \tag{37}$$

where $\tau^c(q)$ is a periodic (position dependent) force ripple induced by commutation errors, while $\tau^o(q)$ denotes periodic force ripples caused by offsets and asymmetries in the actuation devices. Note that if $\epsilon > 0$ is known and constant it can easily be inverted. Obviously for precise trajectory tracking the controller has to reject the input disturbances $d(q,\dot{q})$ which is challenging since the frequency of the periodic force ripples scales with the mover velocity. A detailed discussion on that can be found in [9]. Consequently, all disturbances discussed above appear at the control input, where the influence on the overall system turns out strong.

Finally Fig. 7 depicts simulation results in y-direction of the overall motion stage model compared to experimental step response data. Clearly, the influence of external forces can be recognized by the waviness of the position signals. However, the overall model match is nearly perfect and very well suited for controller design.

IV. CONCLUSION AND FUTURE WORK

In this work we derived an accurate yet simple model of a planar precision positioning system that is capturing all the relevant dynamics. We investigated different kinds of disturbances, while proposing phenomenological models in order to have a suitable description at hand. In conclusion, the overall model applies for the whole traversing range on the x and y axes and the entire input current/force range where it turns out suitable to a very large degree of precision. From the structural point of view, the motion stage can be seen as a simple, linear Euler-Lagrange system with state dependent and periodic (sinusoidal) input disturbances. The derived model may be considered to serve well as a basis for analysis, design and the assessment of advanced control algorithms. This will be part of future work/investigations.

REFERENCES

[1] S. Devasia, E. Eleftheriou, and S. Moheimani, "A survey of control issues in nanopositioning," *IEEE Transactions on Control Systems Technology*, vol. 15, no. 5, pp. 802–823, 2007.

[2] P. Bolognesi, O. Bruno, A. Landi, L. Sani, and L. Taponecco, "Electromagnetic actuators featuring multiple degrees of freedom: a survey," in *Int. Conf. on Electrical Machines (ICEM 2004), Cracow, Poland*, 2004.

[3] T. Chung, C. Chu, K. Fan, J. Yen, and K. Szu, "Development of a nano-positioning planar motion stage," in *2nd Int. Conf. on Mechanical and Electronics Engineering (ICMEE)*, vol. 1, 2010, pp. 122–126.

[4] S. Dejima, W. Gao, K. Katakura, S. Kiyono, and Y. Tomita, "Dynamic modeling, controller design and experimental validation of a planar motion stage for precision positioning," *Precision engineering*, vol. 29, no. 3, pp. 263–271, 2005.

[5] Y. Tomita, Y. Koyanagawa, and F. Satoh, "A surface motor-driven precise positioning system," *Precision engineering*, vol. 16, no. 3, pp. 184–191, 1994.

[6] S. Dian, Y. Arai, and W. Gao, "Dynamic compensation of modeling uncertainties and disturbances of a precision planar motion stage based on sliding mode observer," *Int. Journal of Advanced Manufacturing Technology*, vol. 46, no. 9, pp. 899–912, 2010.

[7] W. Gao, S. Dejima, H. Yanai, K. Katakura, S. Kiyono, and Y. Tomita, "A surface motor-driven planar motion stage integrated with an xyθ_z surface encoder for precision positioning," *Precision Engineering*, vol. 28, no. 3, pp. 329–337, 2004.

[8] K. Tan, K. Tang, H. Dou, and S. Huang, "Development of an integrated and open-architecture precision motion control system," *Control Engineering Practice*, vol. 10, no. 7, pp. 757–772, 2002.

[9] C. Röhrig, "Optimal commutation law for three-phase surface-mounted permanent magnet linear synchronous motors," in *45th IEEE Conference on Decision and Control*, 2006, pp. 3996–4001.

[10] M. Hamers, "Actuation principles of permanent magnet synchronous planar motors: a literature survey," Tech. Rep. CBT 534-05-2717 DCT 2005.149, Philips Applied Technologies, Eindhoven, Tech. Rep., 2005.

[11] M. Khan, N. Bencheikh, C. Prelle, F. Lamarque, T. Beutel, S. Büttgenbach, *et al.*, "A long stroke electromagnetic xy positioning stage for micro applications," *IEEE/ASME Transactions on Mechatronics*, pp. 1–10, 2011.

[12] E. Furlani, *Permanent magnet and electromechanical devices: materials, analysis, and applications*. Academic Press, 2001.

[13] J. Chiasson, *Modeling and high performance control of electric machines*. John Wiley & Sons, 2005.

[14] I. Compter, "Electro-dynamic planar motor," *Precision Engineering*, vol. 28, no. 2, pp. 171–180, 2004.

[15] S. Ruben and T. Tsao, "Optimal commutation laws by real-time optimization for multiple motor driven systems," in *American Control Conference*, 2010, pp. 1942–1947.

[16] T. Fossen, *Guidance and control of ocean vehicles*. John Wiley & Sons, 1994.